Hardwood lignin pyrolysis in the presence of nano-oxide particles embedded onto natural clinoptilolite

Nevenka Rajić, Nataša Zabukovec Logar, Aleksander Rečnik, Mohamad El-Roz, Frederic Thibault-Starzyk, Paul Sprenger, Lenka Hannevold, Anne Andersen, Michael Stöcker

Hardwood lignin pyrolysis in the presence of nano-oxide particles embedded onto natural clinoptilolite

Nevenka Rajic´ [a,⇑], Nataša Zabukovec Logar [b], Aleksander Recˇnik [c], Mohamad El-Roz [d], Frederic Thibault-Starzyk [d], Paul Sprenger [e], Lenka Hannevold [e], Anne Andersen [e], Michael Stöcker [e]

[a] Faculty of Technology and Metallurgy, University of Belgrade, Karnegijeva 4, 11000 Belgrade, Serbia [b] National Institute of Chemistry, Hajdrihova 19, 1000 Ljubljana, Slovenia
[c] Jozef Stefan Institute, Jamova 9, 1000 Ljubljana, Slovenia
[d] Laboratoire Catalyse & Spectrochimie, ISMRA-CNRS, Boulevard Maréchal Juin 6, 14050 Caen, France [e] SINTEF Materials and Chemistry, P.O. Box 124 Blindern, 0314 Oslo, Norway

Abstract

In this study the catalytic activity of Na-rich and MO-containing natural clinoptilolite (MO – nanoparticles of NiO, ZnO, or Cu_2O) were studied in the pyrolysis of hardwood lignin. The clinoptilolite samples exhibit different catalytic activities which depend mainly on type of the nano-oxide. The presence of nano-oxides did not affect theporosity of the clinoptilolite framework but influenced its acidity. However, it seems that acidity of the lattice did not influence the catalytic activity of the clinoptilolite in the pyrolisis of hardwood lignin. The number of Lewis acid sites increased significantly for ZnO- and Cu_2O-containing clinoptilolite whereas for the NiO-sample it did not change appreciably in comparison to the parent zeolite. The amount of phenols in the as-produced bio-oil varies from 39% for ZnO-clinoptilolite, 43% for Na-rich clinoptilolite, to 50 and 54 % for Cu_2O- and NiO-containing samples, respectively. The highest yield of phenols obtained in the presence of NiO-containing clinoptilolite is ascribed to a synergetic interaction of the clinoptilolite lattice and nano-NiO particles.

Keywords: clinoptilolite, pyrolysis, lignin, bio-oil, catalysis

1. Introduction

Lignocellulosic biomass is the most abundant renewable material which is a potential feedstock for producing chemicals, fuels and materials. It has recently been reported that between 40 and 50 million tons per year are produced in the world mostly as a non-commercialized product [1]. Although most research in the area of the potential uses of lignin is focused on the pyrolysis process for lignin treatment, investigations on the use of lignin in the production of phenols are rather scarce [1].

Among various biomass conversion processes, pyrolysis has long been known to yield an oil-like liquid (i.e. “bio-oil”) which can be used either directly or as an energy carrier product. In the biomass pyrolysis the presence of heterogeneous catalysts, such as metal oxides, molecular sieves and active carbon, plays a critical role [2, 3]. Recently, it has been reported that the use of NiO particles decreases the decomposition temperature of biomass components, such as cellulose, xylan and lignin [4]. Since nano-sized particles are not thermodynamically stable, which results in the loss of catalytic activity of the catalysts, porous materials have been employed as the matrix for nano-oxides in order to maintain the catalyst`s activity for a longer period [5].

On other hand, clinoptilolite material is one of the most abundant natural zeolites with intersecting, open channels occupied by hydrated ion-exchangeable cations which are potentially active catalytic sites [6]. Their thermal stability allows its use in a wide temperature range in a catalytic application. Recently, we have found that a complete dehydration of supported Ni(II)-, Cu(II)- and Zn(II) on clinoptilolite support leads to the formation of corresponding oxides with nanometric size [7]. Therefore, clinoptilolite could be used as good support to immobilize the nano-oxide particles.

In this work we will presents the immobilization of several nano-oxides onto the natural clinoptilolite surface. The samples have been characterized using XRD, N_2-sorption and IR spectroscopy. The catalytic activities of the samples have been tested and discussed the lignin pyrolisis reaction.

2. Experimental

2.1. Preparation of catalysts

A natural zeolite (Z) obtained from the sedimentary Zlatokop deposit (Vranjska banja, Serbia) was used in the experiments. In order to improve the zeolite exchange capacity the zeolitic tuff was first converted into the Na-form (NaZ) by treating Z with 2 mol dm^{-3} of NaCl solution at 25 °C for 48 h. Prior to its further use, the NaZ was filtered off from the suspension, washed with distilled water until it was free of chloride ions and dried at 105 °C. This conversion does not affect the crystallinity of the Z.

The ion-exchange was performed at 35 °C using NaZ and 6-mmol dm^{-3} MCl_2 (M – Ni, Cu, Zn) solution in a ratio of 1g (solid)/100 cm^3 (solution). Metal-containing products were then recovered by filtration. XRPD analysis confirmed that the treatments did not affect crystallinity of the clinoptilolite lattice. Elemental analysis of the clinoptilolite phase of Z, NaZ, Ni-NaZ, Cu-NaZ and Zn-NaZ are given in Table 1.

The metal-loaded samples of Ni-NaZ, Cu-NaZ and Zn-NaZ containing (wt.%) 0.78 Ni^{2+}, 2.07 % Cu^{2+} or 1.18 Zn^{2+} were heated at a heating rate of 10 ^oC min^{-1} to 550 ^oC and then were isothermally heated for 60 min in the air at 550 °C to be completely dehydrated. The obtained products were denoted NiO-NaZ, Cu_2O-NaZ and ZnO-NaZ.

2.2. Characterization methods

An elemental analysis of the natural and modified zeolitic samples was performed using energy dispersive X-ray spectroscopy (EDS) by a scanning electron microscope JEOL JSM-6610LV. The samples were prepared by embedding grains in an epoxy film, polishing the crystallites, cutting with a fine-grid diamond cut and coating with carbon. This careful preparation provided an intersection view of the crystallite grains and allowed for a detailed elemental analysis of the major mineral phases. An average elemental composition of the samples was obtained by a data collection at 10 different mm^2-sized windows on the pellet surface.

Thermal analysis was performed using a SDT Q-600 simultaneous TGA-DSC instrument (TA Instruments). The sample (mass app. 10 mg) was heated in a standard alumina sample pan, the experiment being carried out under air with a flow rate of 0.1 dm^3 min^{-1}.

The crystallinty of the NaZ and M-NaZ (M=Ni, Cu, Zn) samples was studied by XRPD analysis using the data obtained at room temperature on a PANalytical X'Pert PRO diffractometer using CuKα radiation. The data were collected in the 2θ range from 5 to 75º 2Θ in steps of 0.017º 2Θ with a total measurement time of 4 hours.

The dehydrated M-NaZ products (NiO-NaZ, Cu_2O-NaZ and ZnO-NaZ) were analyzed by transmission electron microscopy (TEM) and identification of the obtained oxides was performed using the selected area electron diffraction (SAED) over multiple nano-crystals. TEM studies were performed using a 200-kV TEM (JEM-2100 UHR, Jeol Inc., Tokyo, Japan) equipped with an ultra-high-resolution, objective-lens pole-piece having a point-to-point resolution of 0.19 nm, which is sufficient to resolve the lattice images of the oxide nanoparticles. For the TEM studies, the samples were crushed in an agate mortar, dispersed in absolute ethanol and applied to a Cu-holey carbon grid. From the TEM image, the diameter of the oxide nanoparticles was measured

in order to determine their average size. Due to the relatively small size of the nanoparticles, the selected-area electron diffraction (SAED) was performed over multiple nanocrystals to obtain the characteristic diffraction rings and the structure-specific *d*-values.

The BET surface areas (S_{BET}), the pore volume and the average pore diameter of NaZ and the dehydrated M-NaZ samples were measured by N_2 adsorption at -196 °C using Hiden Isochema HTP1-V Volumetric Analyzer. The samples were previously outgassed in vacuum for 3h at 350 °C. BET specific surface areas were calculated from adsorption data in the relative pressure range p/p_0 from 0.04 to 0.18. The Dubinin-Astakhov analysis was applied to determine the pore size distributions.

The surface acidity of the NaZ and the dehydrated M-NaZ samples were measured by NH_3-temperature programmed desorption (NH_3-TPD) using a Micromeritics AutoChem II 2920 catalyst characterization system. The samples [0.1550(4) g] were first heated to 390 °C (20 °C min^{-1}) and left at that temperature for 120 min. After cooling the material to 100 °C (15 °C min^{-1}), a mixture of 10 % NH_3 and He (25 cm^3 (STP min^{-1}) was passed over the material for 30 min. Subsequently, the material was left under flowing He (25 cm^3 (STP) min^{-1}) for 60 min at 100 °C to remove physisorbed NH_3. NH_3-TPD was performed by ramping the material at 10 °C min^{-1} to 700 °C in He [(25.1 cm^3 (STP) min^{-1}, 10 °C min^{-1}, 30 min at 700 °C]. The ammonia content in the effluent was monitored using a TCD. The total amount of ammonia was quantified by integration of peaks with a Micromeritics' Peak Editor software.

Acid sites were characterized and quantified by pyridine absorption using FTIR spectroscopy. FTIR spectra were recorded with a resolution of 4 cm^{-1} on a Bruker IFS 6/S spectrophotometer equipped with a DTGS detector. The samples were pulverized and pressed into self-supported disks (15 mg; area of 2 cm^2) and placed in a quartz IR cell with KBr

windows. A thermal treatment at 390 °C (20 °C min^{-1}) was carried out in vacuum for 2 h in order to remove physisorbed water. After cooling at room temperature an IR spectrum was recorded (it will be referred to as background). The adsorption of pyridine was then carried out, dosing 5 mbar at equilibrium over the disk for 10 min. A second spectrum was recorded after the removal of physisorbed pyridine by outgassing at 150 °C for 10 min. The characterization of acid sites was effectuated on a difference spectrum obtained by subtraction of the background from the spectrum recorded after the pyridine adsorption.

The interaction of pyridine with the Brønsted and Lewis acid sites of the samples gives rise to bands at 1575-1525 cm^{-1} and 1470-1435 cm^{-1} range, respectively. The concentrations (C) of sites were calculated using the integrated absorbance A of the bands and the molar extinction coefficients ε as measured by Emeis, *i.e.* 2.22 cm μmol^{-1} for Lewis sites and 1.67 cm μmol^{-1} for Brønsted sites [8]. The formula used takes also into account the weight (w_d) and area (s_d) of the disk:

$$C = \frac{A}{\varepsilon} \frac{s_d}{w_d}$$

Pyrolysis products were analyzed by gas chromatography and GC–MS analysis. The gaseous products were analyzed using an Agilent 7890A equipped with a FID and two TCD detectors and a HP-PONA silica capillary column from Agilent, 50 m x 0.20 mm. The liquid products were analyzed by a gas chromatograph Agilent 6890 coupled to a mass selective detector Agilent 5973. A combination of two silica capillary columns was used for the separation: a slightly polar DB-17 from J&W Scientific, 30 m x 0.32 mm, and a nonpolar HP-5 from Agilent, 30 m x 0.25 mm. Helium with a flow rate of 2.5 cm^3 min^{-1} was used as a gas carrier.

2.3. Catalytic test

The lignin pyrolysis experiments were carried out in a bench scale fixed bed reactor under nitrogen atmosphere. The reactor was filled with 0.7 g of catalyst or sea send and covered with 1.5 g of lignin. For all experiments the as-received hardwood lignin (provided by Innventia) was used. The reactor temperature was kept constant at 500 °C, while the time of nitrogen introduction into the reactor was 45 min (flow rate of 100 cm^3 min^{-1} for 15 min and 30 cm^3 min^{-1} for 30 min). The liquid products were collected in a liquid bath (-17 °C) and quantitatively measured in a pre-weighted glass receiver. The bio-oil produced was initially in one phase, and two phases of the liquid – organic and aqueous – were separated with dichloromethane. The gaseous products were collected and measured by water displacement and the amount of the solid residue formed was measured by direct weighting.

The resulting gas and liquid products were analyzed by GC and GC/MS. The compounds were grouped into eight characteristic groups, such as hydrocarbons (mainly aromatics with one aromatic ring), phenols (with one aromatic ring and a hydroxyl group), alcohols, carbonyls (including aldehydes), carboxylic acids, PAHs (polycyclic aromatic hydrocarbons; aromatics with several rings and their derivates), furans and heavy compounds (hydrocarbons and phenols with a molar mass over 152 g/mol).

3. Results

A previous detailed X-ray powder diffraction (XRPD) phase analysis based on quantitative Rietveld refinement showed that the zeolitic tuff contains 72.6 % clinoptilolite phase, 14.6 % feldspar plagioclase and 12.8% quartz [9]. Estimated errors for the phase composition are up to 5 %

for clinoptilolite and feldspars, and for other phases up to 2 %. The transition metal (Ni, Cu, Zn) loading did not affect crystallinity nor dehydration of the metal-loaded samples. This is in accord with the fact that natural clinoptilolite exhibits a high thermal stability [10].

The EDS analysis of the parent zeolitic tuff, its Na-rich form (NaZ) and the transition metal-loaded samples (M-NaZ) showed that Ni(II), Cu(II) and Zn replace only the Na^+ ions in the clinoptilolite phase. The replacement occurs through an ion exchange of Na^+ by the metal ions since the Na concentration decreases by the transition metal uptake. The results are given in Table 1.

Table 1. Average chemical compositions of the clinoptilolite phase of Z, NaZ and M-NaZ (M = Ni, Cu, Zn) obtained by EDS analysis.

Component	Wt.%				
	Z	NaZ	Ni-NaZ	Cu-NaZ	Zn-NaZ
SiO_2	65.7	66.6	66.5	65.7	65.6
Al_2O_3	13.0	12.9	12.7	12.4	12.5
Fe_2O_3	1.48	1.04	1.23	1.12	1.15
Na_2O	0.95	5.34	4.92	3.31	4.22
K_2O	1.33	0.14	0.13	0.12	0.15
CaO	3.08	1.40	1.33	1.28	1.27
MgO	1.41	1.21	1.19	1.08	1.11
MO*	-	-	0.99	2.60	1.47
Loss of ignition**	12.9	11.5	11.2	12.3	12.6

*M – Ni, Cu, or Zn

**Obtained by thermal analysis

All M-NaZ samples display similar TG/DTG curves. As a typical example, the TG/DTG curves of the NaZ and Ni-NaZ sample are shown in Figure 1. It is evident that the DTG curve exhibits the strongest maxium at about 550 ºC, so that this temperature has been chosen as the one at which to perform the dehydration. Heating under isothermal conditions confirmed that a full dehydration occurs at this temperature.

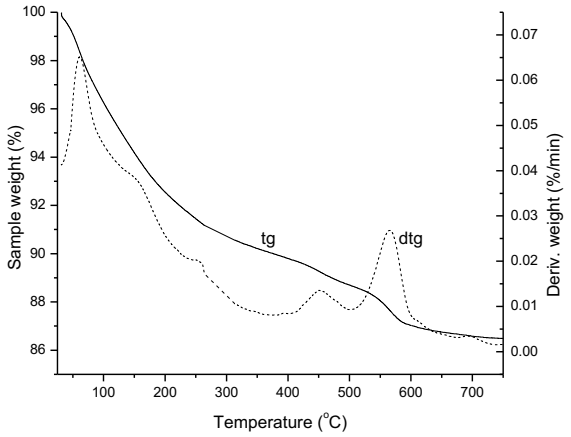

Figure 1. TG/DTG-curves of the Ni-containing sample.

The TEM analysis of the dehydrated products confirms that the clinoptilolite phase did not lose its crystallinty: clinoptilolite phase appears in the form of monoclinic crystalline sheets with well-defined crystal faces (Fig. 2a). Also, the clinoptilolite crystal clusters are populated to

various degrees with spherical nanocrystalline particles, which the SAED analysis revealed to belong to oxides of NiO, Cu_2O and ZnO. The size of the oxide crystallites is between 2 and 15 nm (Fig. 2b). The SAED analysis showed that they belong to the cubic NiO (JCPDF # 78-0643), cuprite Cu_2O (JCPDS 5-667) and wurtzite ZnO structures (JCPDS 00-003-0888).

The size of the oxide particles exceeds the aperture of the largest channel (~ 0.4 nm) in the clinoptilolite lattice, which indicates that the crystallization of the oxide phases occurred at the surface of the clinoptilolite microcystals. It seems likely that during dehydration the metal ions migrate from the channel interior towards the surface where they react with oxygen.

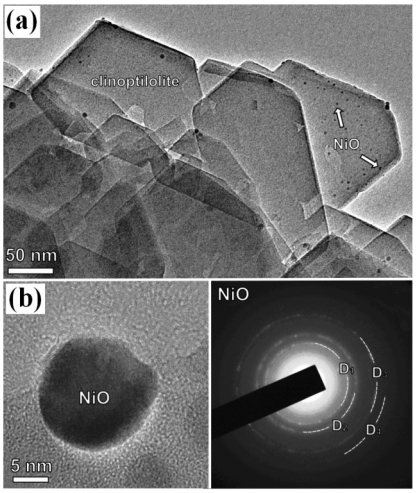

Figure 2. a) TEM image of the NiO-clinoptilolite: Ni-containing clinoptilolite grains with NiO nanoparticles. b) A single NiO particle and the SAED (left) pattern recorded across the NiO particle (right).

The nitrogen adsorption-desorption isotherms at -196 °C revealed that all samples exhibit a type IV isotherm. As a typical example, the N_2 adsorption/desorption isotherms for NiO-NaZ is

presented (Figure 4). Moreover, the calculated BET surface area, and the average pore size diameters for NaZ, NiO-NaZ, Cu_2O-NaZ and ZnO-NaZ are summarized in Table 2. The results indicate that the formation of nano-oxide clusters on the surface of the clinoptilolite phase does not significantly influence the surface area and the accessibility of the pores as compared to the oxide-free NaZ sample. Also, no reliable correlation between the type and the size of the oxide species and the accessible porosity could be established. It should be noticed that nitrogen adsorption isotherm gives only a general insight into the pore volume [10]. Namely, the nitrogen molecule diameter (0.37 nm) is slightly lower than the opening of the eight-membered ring channels (0.33 x 0.46 nm) [11]. Accordingly, from the obtained results one could just conclude that the crystallization of transition metal-oxides does not significantly affect the porosity of the zeolitic tuff.

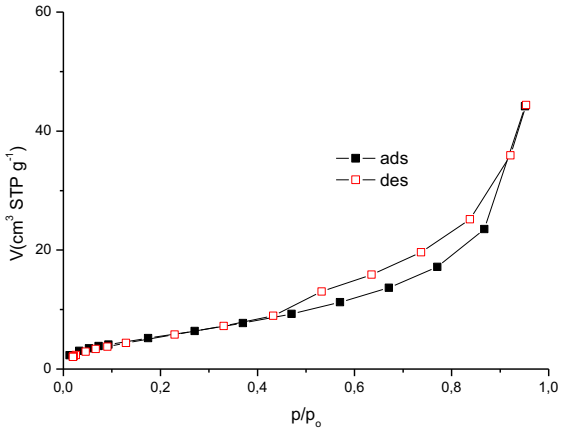

Figure 3. Nitrogen sorption isotherms at -196 °C for the NiO-NaZ sample.

Table 2. S_{BET}, pore volume and pore diameter distribution of NaZ and the MO-containing NaZ samples.

Sample	S_{BET}, $m^2\ g^{-1}$	Average pore diameter, nm
NaZ	27	0.48
NiO-NaZ	32	0.51
Cu_2O-NaZ	31	0.40
ZnO-NaZ	26	0.35

The ammonia-TPD curves of the NaZ and MO-NaZ are shown in Fig. 4. It is evident that the NH_3 release occurs in a broad temperature range indicating the presence of weak and strong acid sites in all samples. According to the literature data, the peak with a maximum below 300 °C corresponds to weak acid sites, which are mainly attributed to the Lewis-type sites [12-14]. The Lewis acid sites are mainly assigned to the extra framework species located in the micropores [12] but also to NH_3 weakly adsorbed on Brönsted acid sites [15]. The peaks with maxima above 300 °C are assigned to strong acid sites attributed to Brönsted-type sites [12, 14]. It should be mentioned that the Brönsted-type sites belong to protons mainly bonded to the aluminosilicate framework although the surface-supported nickel hydroxide has also been reported as a proton donor Brönsted acid [12]. The total number of acid sites of the samples varies from 0.21 to 0.33 mmol g^{-1}.

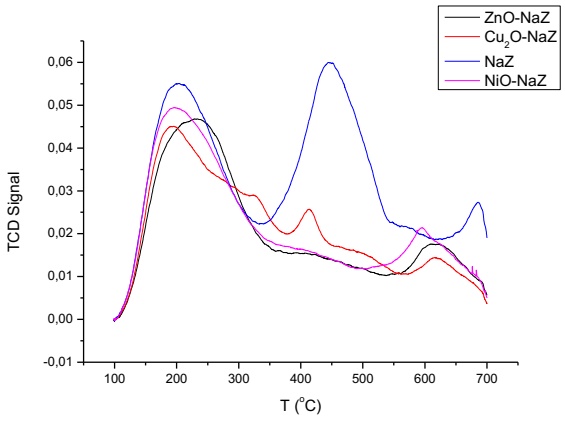

Figure 4. Ammonia TPD profiles for the NaZ, NiO-NaZ, Cu_2O-NaZ and ZnO-NaZ samples. The samples were heated from 100 °C to 700 °C .

To investigate the nature of acid sites, the samples were characterized further by *in situ* FTIR spectroscopy after pyridine chemisorption. Three different bands appeared at 1549, 1490 and 1450 cm^{-1}, strongly supporting the pyridine chemisorption both to Lewis- and Brönsted-type acid sites. The FTIR spectra of NaZ and MO-NaZ are given in Figure 5. The first band is attributed to the interaction between pyridine and the Brønsted-type sites, whereas the third one is assigned to the interaction of pyridine with the Lewis-type sites. The band at 1490 cm^{-1} is due to pyridine adsorbed on both acid types. The areas of the bands at 1549 and 1450 cm^{-1} were used to calculate the concentration of Brönsted and Lewis sites present on the samples. The results are shown in Table 3.

It is evident that the acidity of the samples differs mutually. Firstly, there is an increase of the Lewis- and decrease of Brönsted-type acid sites with the transition metal loading. Secondly, it

is evident that as the amount of transition metals increases the trend becomes more prominent. This is rather unexpected since the formation of transition metal oxides inside the zeolite lattice should generate the Brönsted acidic sites (bridging hydroxyl groups, i.e. Al-OH-Si). The observed phenomenon could be explained by a model of Ward [16]. Namely, according to the model, heating of zeolite above 550 °C leads to a conversion of the Brönsted to Lewis acid sites, *via* generation of one Lewis (electron acceptor) site from two Brönsted acid sites.

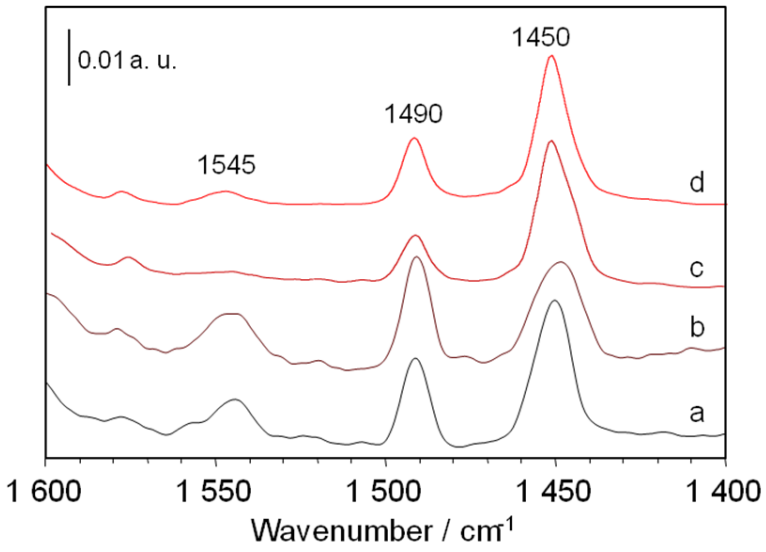

Figure 5. FTIR spectra of NaZ (a) and NiO-NaZ (b) Cu_2O-NaZ (c) ZnO-NaZ (d) samples after pyridine adsorption followed by an evacuation at 50°C under secondary vacuum.

Table 3. Results of quantitative evaluation of the concentration of Lewis and Brönsted acid sites on the samples.

	Area PyL (Abs)	Lewis sites ($\mu mol\ g^{-1}$)	Area PyB (Abs)	Brønsted sites ($\mu mol\ g^{-1}$)	B/L ratio
NaZ	0.237	14.23	0.099	7.904	0.56
NiO-NaZ	0.288	17.30	0.097	7.745	0.45
Cu_2O-NaZ	0.418	46.99	0.043	4.238	0.09
ZnO-NaZ	0.370	41.55	0.041	4.080	0.10

Catalytic tests

Commented [A1]: I think that this part should be more developed whish present the main part of this article!!!

Table 4 gives the composition of the organic phase from the pyrolysis of hardwood lignin in the presence of NaZ and MO-NaZ. For comparison, the results of pyrolysis under similar conditions using an inert solid material (sea sand) are also given in the table. It is evident that presence of all clinoptilolite samples during pyrolysis alters the composition of the organic phase. The yields of phenols are increased in comparison to the non-catalytic test. The increase is most prominent in the presence of NiO-containing NaZ. This sample also significantly reduces the yields of undesirable oxygenated compounds such as organic acids, carbonyls and esters. Moreover, the fraction of toxic polycyclic aromatic hydrocarbons (PAHs) is not significantly increased. This could be attributed to the microporous constrictions of the clinoptilolite lattice which do not promote side-effect catalytic reactions responsible for producing of PAHs (e.g.

cyclization, aromatization etc). As a comparison, MCM-41 catalyst exhibits a catalytic activity in the biomass pyrolysis by increasing the yields of all aromatic compounds, including a 10-fold increase of PAHs. The observed lack of selectivity is attributed to the presence of large pores [17].

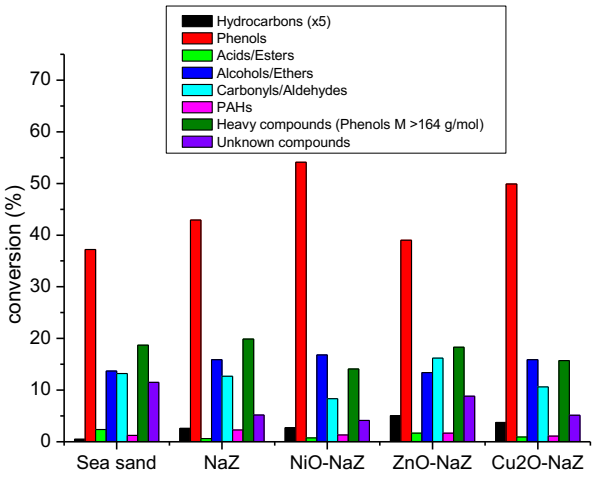

Table 4. Composition of the organic phase from the pyrolysis of hardwood lignin (wt. % of the organic fraction)

	Sea sand	NaZ	NiO-NaZ	ZnO-NaZ	Cu_2O-NaZ
Hydrocarbons	0.10	0.52	0.54	1.01	0.75
Phenols	37.2	42.9	54.1	39.0	49.9
Acids/Esters	2.36	0.62	0.75	1.65	0.93
Alcohols/Ethers	13.7	15.9	16.8	13.4	15.9

Carbonyls/Aldehydes	13.2	12.7	8.34	16.2	10.6
PAHs	1.24	2.27	1.30	1.66	1.10
Heavy compounds (Phenols M >164 g/mol)	18.7	19.9	14.1	18.3	15.7
Unknown compounds	11.5	5.16	4.12	8.82	5.12

Conclusions

Pyrolysis of hardwood lignin in the presence of Na-rich natural clinoptilolite and nano oxide-containing clinoptilolite produced the bio-oil with a high amount of phenols. The highest phenol yield is obtained in the presence of NiO-containing clinoptilolite which indicates that catalytic activity of the natural clinoptilolite in the lignin pyrolisis depends mainly on the type of metal cations present in the zeolitic tuff and not on type of acid sites. The presence of the nano ZnO and Cu_2O in the zeolitic tuff has a significant influence on the acidity of the clinoptilolite framework leading to an increase in the number of Lewis acid sites. This affects the phenol content in the as-produced bio-oil in a different manner. For the Cu_2O-containing clinoptilolite the yield of phenols is increased in comparison to the Na-rich clinoptilolite, whereas for the ZnO-containing sample the increase in the number of Lewis acid sites leads to decrease of the phenols content.

The presence of nano NiO particles in the zeolitic tuff did not considerably change the number and type of acid sites of the clinoptilolite lattice but increased the yield of phenols. This suggests that there is a synergistic interaction between the clinoptilolite lattice and the nano-NiO species in the pyrolisis of hardwood lignin. The results indicate that natural clinoptilolite could be considered as an alternative source for the development of bifunctional catalysts for production of phenols from lignin.

Acknowledgement

The authors gratefully acknowledge the financial support of the Serbian Ministry of Science (project No. 172018) and …...

References:

[1] M. Kleiner and T. Barth, Chem. Eng. Technol. 2008, 31, 736-745

[2] Lin YC, Huber GW. *Energy Environ Sci*, 2009, 2: 68–80;

[3] C. Perego and A. Bosetti, Micropor. Mesopor Mat. 144 (2011) 28-39

[4] Li, R. Yan, B. Xiao, D. Tee Liang, L. Du, Environ. Sci. Techn. 42 (2008) 6224-6229

[5] JF. Li, R. Yan, B. Xiao, DT Liang; DH Lee, Preparation of nano-NiO particles and evaluation of their catalytic activity in pyrolyzing biomass components, Energ Fuel 22 (2008) 16-23.

[6] M. Zabeti, T.S. Nguyen, L. Lefferts, H.J. Heeres and K. Seshan, Bioresource Technol. 118 (2012) 374-381.

[7] N. Rajic, D. Stojakovic, N. Daneu, A. Recnik, J. Phys. Chem. Solids 72 (2011) 800-803.

[8] C.A. Emeis, Determination of Integrated Molar Extinction Coefficients for Infrared Absorption Bands of Pyridine Adsorbed on Solid Acid Catalysts, J. Catal. 141 (1993) 347-354.

[9] S. Cerjan Stefanovic, N.Z. Logar, K. Margeta, N.N. Tusar, I. Arcon, K. Maver, J. Kovac, V. Kaucic, Micropor. Mesopor. Mater. 105 (2007) 251–259.

[10] M. Sprynskyy, R. Golembiewski, G. Trykowski and B. Buszewski, Heterogeneity and hierarchy of clinoptilolite porosity, J. Phys. Chem. Solids 71 (2010) 1269-1277.

[11] Ath. Godelitsas and Th. Armbruster, HEU-type zeolitas modified by transition elements and lead, Micropor Mesopor Mater. 61 (2003) 3-24.

[12] A. Godelitsas et al., Chem. Eur. J 2001, 3705-3721;

[13] A. Ates, Appl. Catal. B: Environmental 76 (2007) 282-290;

[14] T.K. Katranas et al., Micropor. Mesopor. Mat 61 (2003) 189-198]

[15] A. Ates, Characteristics of Fe-exchanged natural zeolites for the decomposition of N_2O and its selective catalytic reduction with NH_3, Appl. Catal. B: Environmental 76 (2007) 282-290.

[16] J.W. Ward, The nature of active sites on zeolites: IV. The influence of water on the acidity of X and Y type zeolites, J. Catal. 11 (1968) 238-250.

[17] E. Antonakou et al., Fuel 85 (2006) 2202-2212